

SCORCH. II. RADIATION-HYDRODYNAMIC SIMULATIONS OF REIONIZATION WITH VARYING RADIATION ESCAPE FRACTIONS

ARISTIDE DOUSSOT,^{1, 2} HY TRAC,² AND RENYUE CEN³

¹*Ecole Normale Supérieure, Département de Physique, 24 rue Lhomond, 75005 Paris, France*

²*McWilliams Center for Cosmology, Department of Physics, Carnegie Mellon University, Pittsburgh, PA 15213*

³*Department of Astrophysical Sciences, Princeton University, Princeton, NJ 08544*

ABSTRACT

For the Simulations and Constructions of the Reionization of Cosmic Hydrogen (SCORCH) project, we present new radiation-hydrodynamic simulations with updated high-redshift galaxy populations and varying radiation escape fractions. The simulations are designed to have fixed Thomson optical depth $\tau \approx 0.06$, consistent with recent Planck observations, and similar midpoint of reionization at $z \approx 7.5$, but with different ionization histories. The modeled galaxy luminosity functions and ionizing photon production rates are in good agreement with recent HST observations. Adopting a power-law form for the radiation escape fraction $f_{\text{esc}}(z) = f_8[(1+z)/9]^{a_8}$, we simulate the cases for $a_8 = 0, 1, 2$ and find that $a_8 \lesssim 2$ in order to have reionization end in the range $5.5 \lesssim z \lesssim 6.5$, consistent with Lyman alpha forest observations. At fixed τ and as the power-law slope a_8 increases, the reionization process starts relatively earlier, ends relatively later, and the duration Δz increases and the asymmetry Az decreases. We find a range of durations $3.1 \lesssim \Delta z \lesssim 3.8$ that is currently in tension with the upper limit $\Delta z < 2.8$ inferred from a recent joint analysis of Planck and South Pole Telescope observations.

Keywords: cosmology: theory - dark ages, reionization, first stars - galaxies: high-redshift - large-scale structure of universe - methods: numerical

1. INTRODUCTION

Cosmic reionization is one of the most significant topic of the modern cosmology with both theoretical and observational issues. The Epoch of Reionization (EoR) is the era of the Universe characterized by the formation of the first stars and galaxies. This emergence takes place in the first billion years of the Universe and leads to a process called reionization. During that process, the neutral hydrogen, which composes the large part of the baryonic matter of the universe, is ionized turning the cold and neutral intergalactic medium (IGM) into a warm and fully ionized area. Yet, some key information about the reionization like the beginning, the end and the duration Δz of that process are still highly unknown.

In the past years, recent observations from the Hubble Space Telescope (HST) and Planck have started to give observational constraints to the EoR. One of that few constraints is the optical depth which is now believed to be $\tau = 0.055 \pm 0.009$ (Aghanim et al. 2016). Starting from that values, it has been deduced that the duration of the reionization should be $\Delta z_{\text{CMB}} < 2.8$ (Adam et al. 2016) if it is assumed that the reionization is completed at redshift $z \approx 6$. Previous studies (e.g. Bouwens et al. 2015b; Finkelstein et al. 2015; Livermore et al. 2017) also tend to show that the main contributors to the reionization are likely to be the early dwarf galaxies of that early universe. However, as the observational frontier has just started to reach the Epoch of Reionization, further analysis and numerical simulation are needed to really precise these constraints.

The project SCORCH (Simulations and Constructions of the Reionization of Cosmic Hydrogen) has been built to give a deeper understanding of the EoR while providing theoretical tools to improve the comparison between observations and theory. On that issue, a further investigation on the effect of distribution and properties of radiation sources and sinks on the reionization process is needed. The RadHydro code (Trac & Pen 2004; Trac & Cen 2007) consists on a N-body + hydro + radiative transfer simulation with subgrid physics shaped on the basis of the latest observations and simulations.

Among the parameters driving the reionization, the galaxy luminosity function (GLF) is one of the less constrained at high redshift. In SCORCH I (Trac et al. 2015), we propose a way to extrapolate the known luminosity function to higher redshift and fainter magnitude. The obtained galaxy function is consistent with the measurements from Bouwens et al. (2015b) and Finkelstein et al. (2015) at redshift $6 \lesssim z \lesssim 10$ and also in good agreement with cosmological simulations (e.g. Gnedin 2016; Feng et al. 2016; Liu et al. 2016; Ocvirk et al.

2016) and semi-analytical models (e.g. Mashian et al. 2015; Mason et al. 2015).

The escape fraction f_{esc} is a numerical parameter that accounts for the fraction of ionizing photons which escapes from the galaxies where they have been created. f_{esc} is therefore physically related to all the internal processes of absorption and emission of photons in the galaxies. As f_{esc} can be computed in many ways, comparison of its value between different works can be difficult. However, there are still some constraints on it and assuming a given GLF with a low-luminosity limiting magnitude $M_{SF} \sim -10.0$ and a galaxy-driven reionization model, $f_{\text{esc}} \gtrsim 0.10 - 0.20$ at $z \gtrsim 6$ (Bolton & Haehnelt 2007). On the contrary, at low-redshift the values obtained from observational measurements are $f_{\text{esc}} \lesssim 0.05 - 0.1$ (Chen et al. 2007; Iwata et al. 2009; Smith et al. 2016) which leads us to consider that f_{esc} varies with the redshift. In Price et al. (2016) both parametric and non-parametric functional forms have been tested to obtain the better expression of f_{esc} . As a result, it appears that f_{esc} can be well-fitted by a simple power-law form whose exponent strongly depends on the value of the optical depth τ that is taken as a reference.

In our current study we pursue the previous works of Trac et al. (2015) and Price et al. (2016) using the SCORCH simulation. We will focus on the influence of the variation of f_{esc} on the duration and the asymmetry of the reionization and on the resulting photoionization and photoheating profile. The other main conclusions deduced from SCORCH like the varying clumping factor or the correlation between the different fields involved will be treated in upcoming papers. In section 2 we discuss the model that we have used for the galaxy luminosity function, the escape fraction and the resulting photoionization rate. The first results of the SCORCH simulation are then presented in Section 3 with our first analysis of them. Section 4 is eventually a summary of our main results. We adopt the concordance cosmological parameters: $\Omega_m = 0.30$, $\Omega_\Lambda = 0.70$, $\Omega_b = 0.045$, $h = 0.7$, $n_s = 0.96$ and $\sigma_8 = 0.8$.

2. METHODS

2.1. *Radiation-Hydrodynamic simulations*

To run our simulations, we use the Radhydro code which has already been used to model both hydrogen and helium reionization (Trac et al. 2008; Battaglia et al. 2013b; La Plante et al. 2017). In order to simultaneously solve collisional gas dynamics, collisionless dark matter dynamics, and radiative transfer of ionizing photons, the Radhydro code combines hydrodynamic and N-body algorithms (Trac & Pen 2004) with an adaptative raytracing algorithm (Trac & Cen 2007). As the ray-

tracing algorithm has adaptive splitting and merging, it improves the resolution and the scaling.

In our study, we run three Radhydro simulations, all starting with the same initial conditions at redshift $z = 300$ and having 2048^3 dark matter particles, 2048^3 gas cells, and up to 12 billion adaptive rays in a comoving box of side length $50 h^{-1}\text{Mpc}$. For each ray we track five frequencies above the hydrogen ionizing threshold of 13.6eV. The nonequilibrium solvers for the ionization and energy equations use the photoionization and photoheating rates computed from the incident radiation flux.

The radiation sources are modelled using an updated subgrid approach. It allows us to match the observed galaxy luminosity functions while controlling the galaxy distributions. Following SCORCH I (Trac et al. 2015), we use a luminosity-accretion rate $L_{\text{UV}}(\dot{M})$ relation inferred from abundance matching to populate dark matter halos with galaxies. By connecting the halo mass accretion rate to the star formation rate, it is then possible to model the episodic nature of high-redshift galaxy formation.

The generation of the halo and galaxy catalogs is done by a particle-particle-particle-mesh (P³M; Trac et al. 2015) N-body simulation with 3072^3 dark matter particles using a high-resolution version of the same initial conditions as the Radhydro simulations. Every 20 million cosmic years, a hybrid halo finder is run on the fly to locate dark matter halos and build merger trees. The particle mass resolution of $3.59 \times 10^5 h^{-1}\text{M}_\odot$ allows the measurement of halo quantities such as mass and accretion rate down to the atomic cooling limit ($T \sim 10^4$ K, $M \sim 10^8 h^{-1}\text{M}_\odot$). See Trac & Gnedin (2011) for a review on reionization simulations.

2.2. Galaxy luminosity functions

The reionization history depends strongly on the abundance of escaped ionizing photons and its evolution. The current observable galaxies with $M_{\text{UV}} \lesssim -17$ and at $z \lesssim 10$ are the sources of only a part of the ionizing photons that have determined the ionization history. To compute the GLF, it is therefore required to extrapolate the known luminosity function to fainter magnitude and higher redshift. We then use the fiducial model that has been created and detailed in SCORCH I (Trac et al. 2015).

Figure 1 presents the overall behaviour of our galaxy luminosity function for the redshift $z \approx 6, 8$ and 10 . The turn-over at fainter magnitude $M_{\text{UV}} \gtrsim 11$ has been determined for this fiducial model in Trac et al. (2015). This limit corresponds to the minimum mass for a dark matter halo to host a galaxy assuming that galaxies

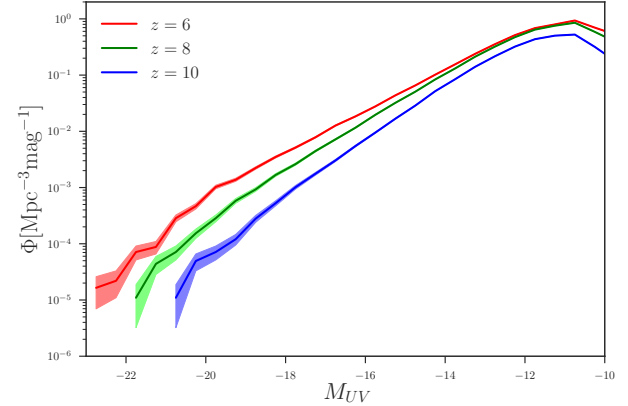


Figure 1. Galaxy luminosity function (binned) as a function of the UV magnitude at $z \approx 6$ (red), $z \approx 8$ (green) and $z \approx 10$ (blue) as obtained during the SCORCH simulation.

are formed only in halos where the gas cools efficiently through atomic transitions.

The galaxy luminosity for $z \approx 6, 8$ and 10 as obtained during the simulation is shown in Figure 2. We truncate the curves before the star formation limit and also show the observational measurements at $z \approx 6$ (Finkelstein et al. 2015; Bowler et al. 2015; Bouwens et al. 2015b, 2017), at $z \approx 8$ (Finkelstein et al. 2015; Bouwens et al. 2015b) and at $z \approx 10$ (Bouwens et al. 2015b, 2016; Oesch et al. 2017). The GLF appears to be consistent with the observational constraints at $z \approx 6$ and $z \approx 8$. In the case of $z \approx 10$, our luminosity function is still consistent with the observational results but has a larger amplitude at low M_{UV} than expected from the observational measurements. However the uncertainties on the measurements at $z \approx 10$ are high and our result matches the theoretical expectation from SCORCH I (Trac et al. 2015).

2.3. Radiation escape fractions

In Price et al. (2016) we found that the new estimations of τ (Ade et al. 2016; Aghanim et al. 2016) implies a generic redshift evolution in the radiation escape fraction $f_{\text{esc}}(z)$. Moreover, a simple parametric form can be used to fit that evolution. Following these conclusions, we then chose a two-parameter single power-law

$$f_{\text{esc}}(z) = f_8 \left(\frac{1+z}{9} \right)^{a_8} \quad (1)$$

where f_8 is the value of the escape function at $z = 8$. In our study, we compare the cases where $a_8 = 0, 1$ and 2 mainly to have a better understanding on the effect of that escape fraction on the reionization history.

The last measurements of the optical depths of Adam et al. (2016) and Aghanim et al. (2016) are respectively

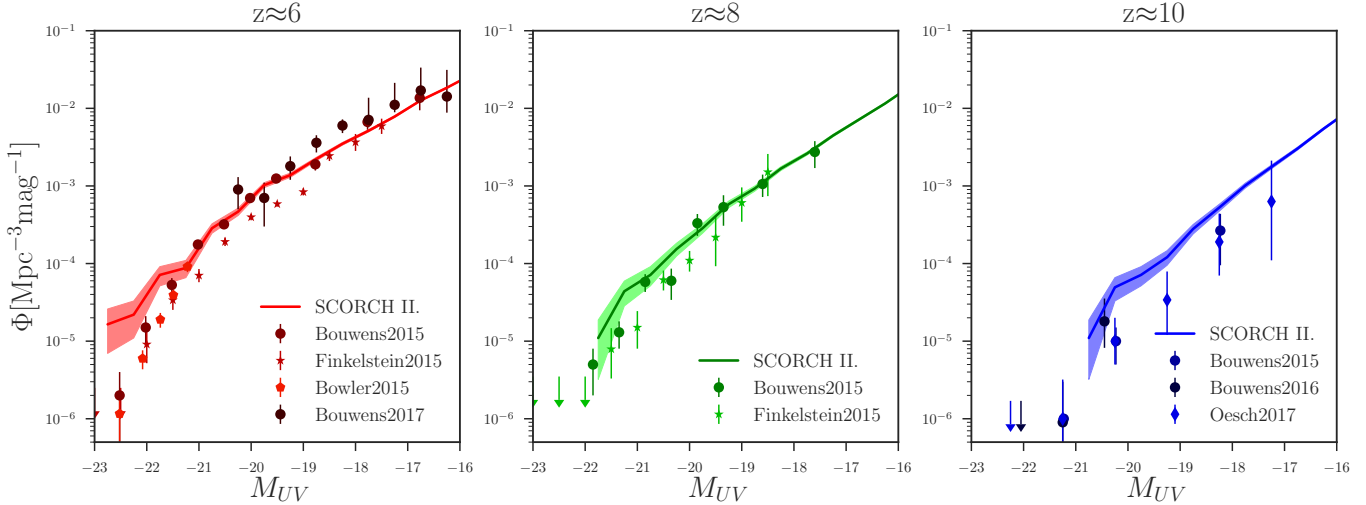


Figure 2. Galaxy luminosity function (binned) as a function of the UV magnitude at $z \approx 6$ (red), $z \approx 8$ (green) and $z \approx 10$ (blue) as obtained for the SCORCH simulations. For comparison, we show the binned observational measurements at $z \approx 6$ (Finkelstein et al. 2015; Bowler et al. 2015; Bouwens et al. 2015b, 2017), at $z \approx 8$ (Finkelstein et al. 2015; Bouwens et al. 2015b) and at $z \approx 10$ (Bouwens et al. 2015b, 2016; Oesch et al. 2017). For $z \approx 6$ and $z \approx 8$ our results are in agreement with the observational values and are still consistent with the uncertain observations for $z \approx 10$.

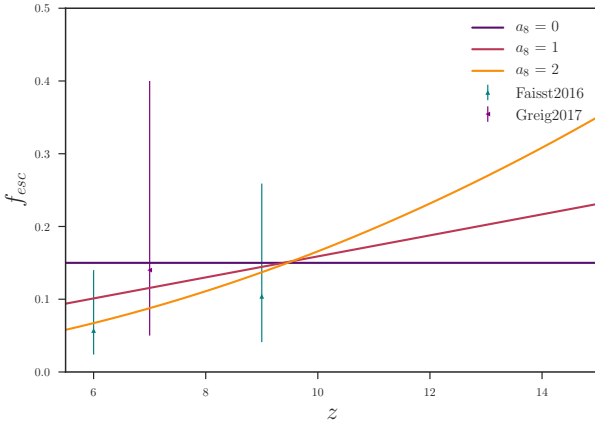


Figure 3. The escape fraction as a function of redshift following the Equation 1 for our three models. The observationally-based predictions of Faisst (2016) and Greig & Mesinger (2017) are shown for comparison.

$\tau = 0.058 \pm 0.012$ and $\tau = 0.055 \pm 0.009$. These values imply that the universe must be half-ionized at $z \approx 8$ and by assuming that the reionization ends before $z \approx 5.5$, the exponent a_8 in Equation 1 is likely to be $0 \lesssim a_8 \lesssim 2$.

Figure 3 shows the behaviour of f_{esc} as a function of the redshift for three typical values of a_8 . The parameter f_8 have been selected for the models to eventually match the value $\tau \approx 0.06$ which we choose to respect the two measurements. Our three models are consistent with the latest predictions from Faisst (2016) and are in good agreement with Greig & Mesinger (2017). Moreover,

the overall normalization of f_{esc} is degenerate with other parameters such as the overall normalization of the GLF and galaxy spectral energy distributions (SED) which may lead to some differences between different studies. Our models then broadly respect the expected escape fraction profile.

2.4. Ionizing photons

The measurement of the photoionization rate $\dot{n}_\gamma(z)$, or of its integral the cumulative ionizing photon number density $n_\gamma(>z)$, is made using the fraction of photons which have escaped from their original galaxy. The photoionization rate is then related to f_{esc} through :

$$\dot{n}_\gamma(z) = f_{\text{esc}} \times \dot{n}_{\gamma,\text{total}}(z). \quad (2)$$

For our approach we use the following formula for the production rate of ionizing photon of Population II star (Trac et al. 2015):

$$\dot{N}_\gamma \approx 10^{46.2 - 0.4M_{UV}} s^{-1} \approx 10^{25.5} s^{-1} \left(\frac{L_{UV}}{\text{erg s}^{-1} \text{Hz}^{-1}} \right) \quad (3)$$

where the conversion between UV magnitude and luminosity has been made with the standard AB relation,

$$M_{UV} = -2.5 \log \left(\frac{L_{UV}}{4.345 \times 10^{20} \text{ erg s}^{-1} \text{Hz}^{-1}} \right) \quad (4)$$

It is worth noting that Equation 3 can be different from the one used in other works (Trac et al. 2015) because of the normalization which is uncertain at a factor

of approximatively 2. Again, it emphasizes that we can only carefully compare our functional form of f_{esc} with some observational constraints as these constraints are derived from a different computation of $\dot{n}_\gamma(z)$. However, we hereby confront our results for $\dot{n}_\gamma(z)$ and its cumulative $n_\gamma(>z)$ to another work from Bouwens et al. (2015a) as they do not depend on an arbitrary choice in their definition.

In Figure 4, we show the evolution of the photoionization rate per hydrogen atoms and of the cumulative ionizing photon number density per hydrogen atoms as functions of the redshift z for our three models of escape fraction. We show that our results differ with the one from Bouwens et al. (2015a) where a constant clumping factor of 3 is considered. It may be due to the fact that, in our study the clumping factor is not fixed and varies with the redshift resulting in a clumping factor always greater than 3. Moreover, the photoionization rate from Bouwens et al. (2015a) does not come from a simulation but from an analytical computation, a calculation that we have also done with our varying clumping factor in Doussot et al. (in prep.).

3. RESULTS

3.1. Optical depth

Figure 5 shows the obtained optical depth τ for our three models as a function of the redshift. The observational measurements of Adam et al. (2016) and Aghanim et al. (2016), which are respectively $\tau = 0.058 \pm 0.012$ and $\tau = 0.055 \pm 0.009$, are also shown for comparison. Our models are in agreement with the measurements and we obtain results near $\tau \approx 0.06$ as we planned to obtain by construction. However, if all of our models are consistent with the observational results, their temporal evolutions of τ are not similar which means that the reionization history is different for each one of them.

3.2. Ionization history

In Figure 6, we show the volume and mass weighted ionization history, respectively $\langle x_{\text{HII}} \rangle_V$ and $\langle x_{\text{HII}} \rangle_M$, for the different studied forms of f_{esc} . We also show some of the latest results obtained from Lyman- α measurements (Schroeder et al. 2013; McGreer et al. 2014; Tilvi et al. 2014; Konno et al. 2017; Ota et al. 2017) and from Planck observations with a constraint on the end of the reionization before $z \approx 6$ (Adam et al. 2016). Our results are generally in agreement with most of the experimental results cited in Figure 6 and no strong contradictions seem to appear.

Figure 7, which presents slice of the reionization-redshift field for our three models, gives a first understanding of the spatial behaviour of the reionization pro-

| Model | $z_{0.5}$ | Δz_{50} | Δz_{90} | Az_{50} | Az_{90} |
|-----------|-----------|-----------------|-----------------|-----------|-----------|
| $a_8 = 0$ | 7.63 | 1.43 | 3.79 | 1.64 | 3.09 |
| $a_8 = 1$ | 7.51 | 1.77 | 4.53 | 1.64 | 2.99 |
| $a_8 = 2$ | 7.30 | 2.33 | 5.61 | 1.59 | 2.71 |

| Model | $t_{0.5}$ | Δt_{50} | Δt_{90} | At_{50} | At_{90} |
|-----------|-----------|-----------------|-----------------|-----------|-----------|
| $a_8 = 0$ | 7.27 | 1.74 | 3.90 | 1.34 | 1.88 |
| $a_8 = 1$ | 7.43 | 2.21 | 4.72 | 1.27 | 1.65 |
| $a_8 = 2$ | 7.71 | 3.09 | 6.21 | 1.13 | 1.28 |

Table 1. Characterizing values of each model using the volume-weighted ionization history. For the second table, $t_{0.5}$, Δt_{50} and Δt_{90} are expressed in 10^8yr .

cess. We show that the reionization has the same spatial behaviour for our three models. The region around the galaxies are ionized first by the sources, the ionization grows until the whole universe is reionized and ends in the underdense cold intergalactic medium. Figure 7 also emphasizes a strong difference between the cases as the reionization in case $a_8 = 0$ seems to have occurred in a shorter time-scale than for the two other cases whereas the reionization in the case $a_8 = 2$ appears to extend itself in a larger time-scale.

3.3. Duration and asymmetry

We hereby confirm that the main effect of the variation of the exponent of the escape fraction is to change the duration of the reionization. It is hard to measure from simulations the physical processes at the very beginning and the very end of the reionization. Thus, we define two durations

$$\Delta z_{50} \equiv z_{0.25} - z_{0.75} \quad (5)$$

$$\Delta z_{90} \equiv z_{0.05} - z_{0.95} \quad (6)$$

where $z_j \equiv z(x_{\text{HII}} = j)$, to express the duration of the reionization like in some previous work (Zahn et al. 2012; Battaglia et al. 2013b). To better characterize the reionization history, we also define the asymmetry as following:

$$Az_{50} \equiv \frac{z_{0.25} - z_{0.5}}{z_{0.5} - z_{0.75}} \quad (7)$$

$$Az_{90} \equiv \frac{z_{0.05} - z_{0.5}}{z_{0.5} - z_{0.95}} \quad (8)$$

Table 1 presents the characterizing values of each model which emphasize the differences between their reionization histories. We see that the duration of the reionization is longer when the exponent a_8 in the power-law fit of f_{esc} is larger. Moreover, these values suggest

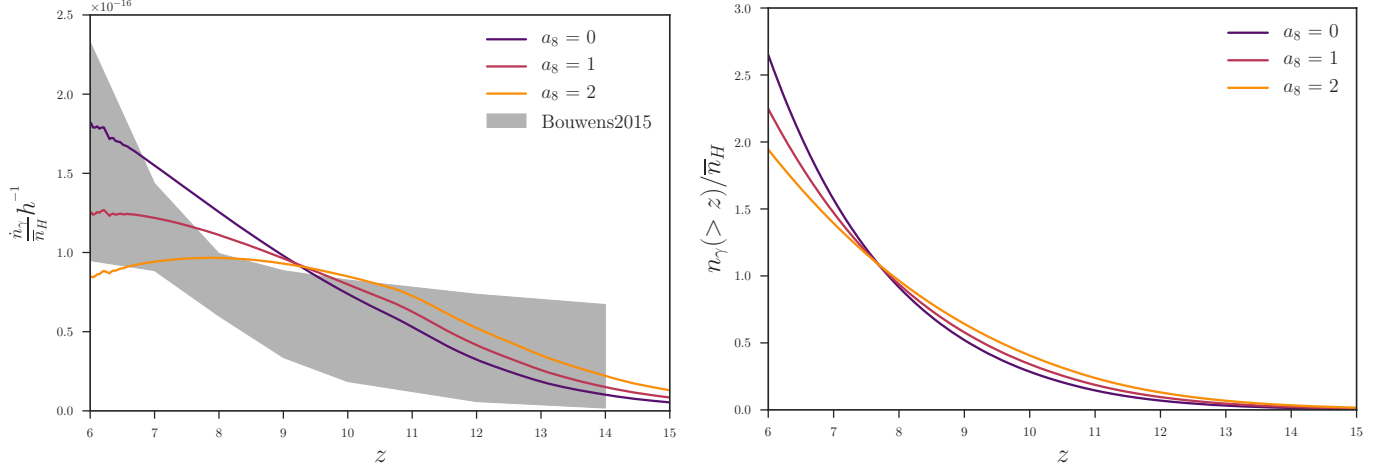


Figure 4. Photoionization rate per hydrogen atoms (left) and cumulative ionizing photon number density per hydrogen atoms (right) as functions of the redshift z for our three functional forms of f_{esc} with $a_8 = 0$ (red), $a_8 = 1$ (blue) and $a_8 = 2$ (green). We show for comparison the observational results, based on HST observations, from Bouwens et al. (2015a) (shaded grey) which considers a constant clumping factor.

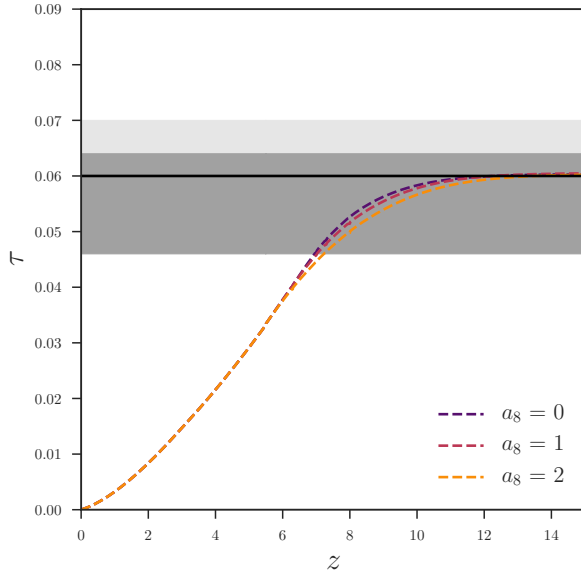


Figure 5. Optical depth as a function of the redshift for our three forms of f_{esc} . The optical depth of $\tau = 0.058 \pm 0.012$ from Adam et al. (2016) (light grey) and $\tau = 0.055 \pm 0.009$ from Aghanim et al. (2016) (dark grey) are shown for comparison. The optical depths of our three models are in agreement with both measurements.

a simple relation for $\Delta z(a_8)$ and $Az(a_8)$ even if other simulations with $0 \lesssim a_8 \lesssim 2$ are needed to determine it.

From Table 1 we also observe that, in any case, there is a non-negligible asymmetry on the duration of the part of the reionization before and after $x_{\text{HII}} = 0.5$. The asymmetry is even larger when we consider a larger interval of the reionization history (i.e. $0.05 \leq x_{\text{HII}} \leq 0.95$ instead of $0.25 \leq x_{\text{HII}} \leq 0.75$). For our three simula-

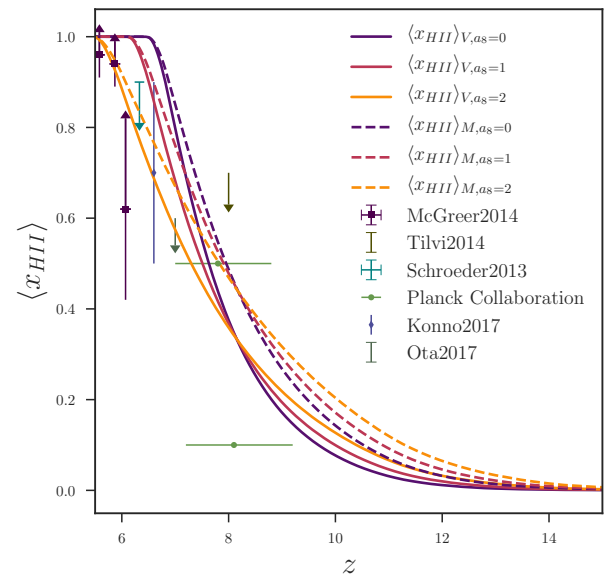


Figure 6. Volume weighted (continuous) and mass weighted (dash) ionization fraction as a function of redshift for the three presented models with $z(x_{\text{HII}} = 0.5) \approx 8$. We show the latest results inferred from Lyman- α measurements (Schroeder et al. 2013; McGreer et al. 2014; Tilvi et al. 2014; Konno et al. 2017; Ota et al. 2017) and from Planck observations with the constraint $z(x_{\text{HII}} = 0.99) > 6$ (Adam et al. 2016).

tions we then have that the first-half of the reionization ($x_{\text{HII}} < 0.5$) is longer than the latter-half ($x_{\text{HII}} > 0.5$). It can be explained by the fact that the photoionization rate \dot{n}_γ (shown in Figure 4) gradually increases for a decreasing redshift. Hence, at the beginning of the reion-

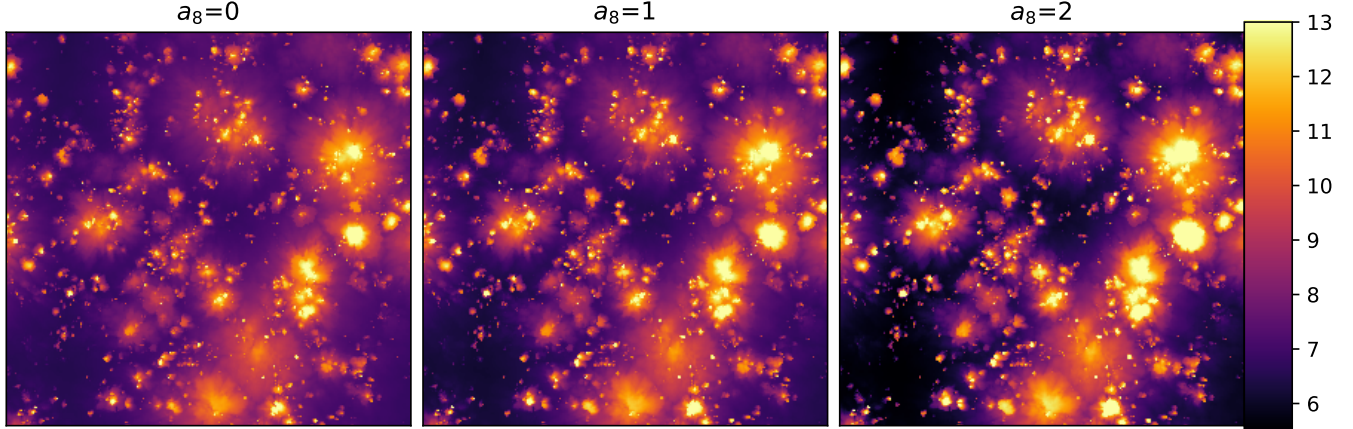


Figure 7. Image of a slice of size $(50 h^{-1}\text{Mpc})^2$ of the reionization-redshift field (the value of one cell is the redshift when it has been ionized) for both of our three models at the end of the reionization.

ization, the photoionization rate is at its lowest values explaining why the ionization process is slow.

We also show that if Δz increases for an increasing a_8 , the asymmetry decreases for an increasing a_8 . It is consistent with the temporal evolution of f_{esc} and of \dot{n}_γ shown in Figures 3 and 4 because the more the escape fraction is high at the beginning of the reionization, the more the number of ionizing photons escaping the galaxy is large and so the more the ionization process is quick. Moreover the photoionization in the model $a_8 = 2$ is higher than in the two other models at high redshift and lower at low redshift. It implies an acceleration of the reionization at the beginning and a slowdown of the process at the end.

The duration of the reionization is also inferred in the Planck Collaboration (Adam et al. 2016) based on a joint analysis using the South Pole Telescope (SPT) measurements of the patchy kinetic Sunyaev-Zeldovich (KSZ; Sunyaev & Zeldovich 1970; Ostriker & Vishniac 1986) effect angular power spectrum at $l=3000$ (George et al. 2015) and only our theoretical models from Battaglia et al. (2013a). Assuming that $z_{0.99} > 6$,

$$\Delta z_{\text{CMB}} \equiv z_{0.1} - z_{0.99} < 2.8 \text{ (95\% confidence)} \quad (9)$$

However this result depends on the assumptions made in the analysis and modelling of the patchy KSZ angular power spectrum. Using the definition 9 of the duration, we obtain the results presented in Table 2.

Our model $a_8 = 2$ does not match the constraint $z_{0.99} > 6$ as it can be seen in Table 3 but the two other models do respect it. Accordingly, our theoretical predictions and the observational constraints from the Planck Collaboration are currently in tension.

3.4. Temperature

| a_8 | 0 | 1 | 2 |
|-------------------------|-----|-----|-----|
| Δz_{CMB} | 3.1 | 3.8 | 4.8 |

Table 2. Duration of the reionization obtained from SCORCH simulation with the definition of Adam et al. (2016) for the three models $a_8 = 0, 1$ and 2.

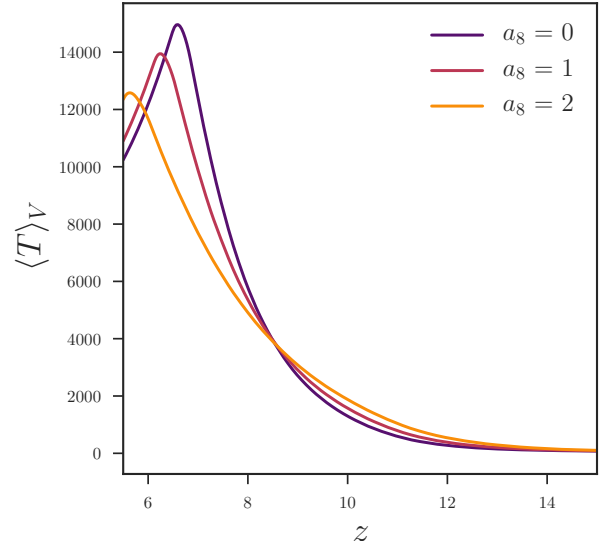


Figure 8. Volume weighted average temperature $\langle T \rangle_V$ as a function of redshift for the three models.

Like the photoionization, the photoheating is also impacted by the evolution of the radiation. Figure 8 presents the volume weighted average temperature $\langle T \rangle_V$ as a function of redshift for the three models. At $z \gtrsim 8.5$ we can see that the photoheating process is more advanced in the model $a_8 = 2$ following the fact that the ionization fraction is higher in this case at this redshift.

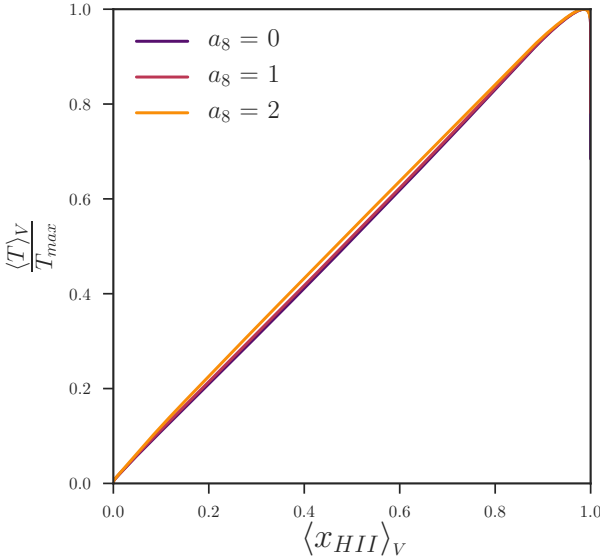


Figure 9. Normalized volume weighted average temperature of the sampling box as a function of the volume weighted ionization fraction of hydrogen $\langle x_{HII} \rangle_V$ for the three models.

On the contrary, at $z \lesssim 7.5$, the temperature in the model $a_8 = 0$ is higher than in the other models because of the fact that the ionization is higher for this model at this redshift. We also show that the maximal temperature is higher in the model $a_8 = 0$. It is due to the shorter duration of the reionization Δz which implies that the effect of the adiabatic cooling process during the reionization, due to the universe expansion, is smaller than it could have been on a longer period.

After the end of the ionization process, in all cases, the photoheating process cannot stabilize the temperature at its higher values leading to a cooling of the gas. That cooling is in a more advanced state in the model with $a_8 = 0$ than in the other because the reionization ended up early giving to the gas more time to cool.

Despite their differences, the underlying physical process in all models is the same. In Figure 9, we show the normalized volume weighted average temperature of the sampling box as a function of the volume weighted ionization fraction of hydrogen $\langle x_{HII} \rangle_V$. Analyzing $\langle T \rangle_V$ as a function of $\langle x_{HII} \rangle_V$ and normalizing it by its maximal value allow us to cancel the influence of the different durations of the reionization Δz of the models to just focus on the physical evolution of the photoheating process when it is started. As the behaviour is strictly the same for all models, the fact that the underlying physical process is the same is therefore endorsed. We also show a nearly linear dependency between $\langle T \rangle_V$ and $\langle x_{HII} \rangle_V$ with a coefficient of proportionality of the order of 1.

We show in Figure 10 the temperature distribution of the same slice of our sampling box at the same redshift for our three different models to give a first insight of the spatial distribution of the temperature. By referring to these temperature fields, we can confirm that the temperature evolution in the universe is strongly linked to the reionization history and so changes with the assumed functional form of the escape fraction. At $z \approx 9.5$ the increase of the temperature, revealing the position of the ionization front, is located around the sources where the reionization has started. At $z = 5.5$ it is worth noting that, in all models, the gas in the vast underdense intergalactic medium is hotter than the high density gas closer to the sources. As previous works has emphasized it (e.g. Trac et al. 2008), it is because the gas in the intergalactic medium has been ionized later than the gas around the sources that the former has less time to cool than the latter. A broader study of the spatial distribution of the temperature and its heterogeneity depending on the density of the gas will be done in a future work.

4. CONCLUSION

The new RadHydro simulations based on the works of Trac et al. (2015) and Price et al. (2016) allow us to have a better understanding of the Epoch of Reionization and of the global behaviour of the parameters that constraint that epoch. In this study, we have presented the first main results of that simulation for three different cases. These cases come from the form of the escape fraction f_{esc} which has been fitted as a simple power-law form and which has been shaped in three different ways: to be constant ($a_8 = 0$) as assumed in most previous works, to vary linearly ($a_8 = 1$) and to vary quadratically ($a_8 = 2$).

Each of these models matches the observational values of the optical depth τ from Adam et al. (2016) and Aghanim et al. (2016) and are then consistent with the observations. Based on these cases, we can isolate the f_{esc} dependency of the reionization history. We concluded that the duration of the reionization Δz increases with the increase of the exponent of the escape fraction's power-law. On the contrary the asymmetry Az between the beginning and the end of the reionization decreases with the increase of that exponent. However, our duration of the reionization conflicts with the result from Adam et al. (2016) which leads us to consider that more studies are needed.

In term of the photoheating, we pointed out that the increase in temperature happens during the ionization process, and then that there is a correlation between the temperature and the reionization history. We have also shown that the maximum value of the tempera-

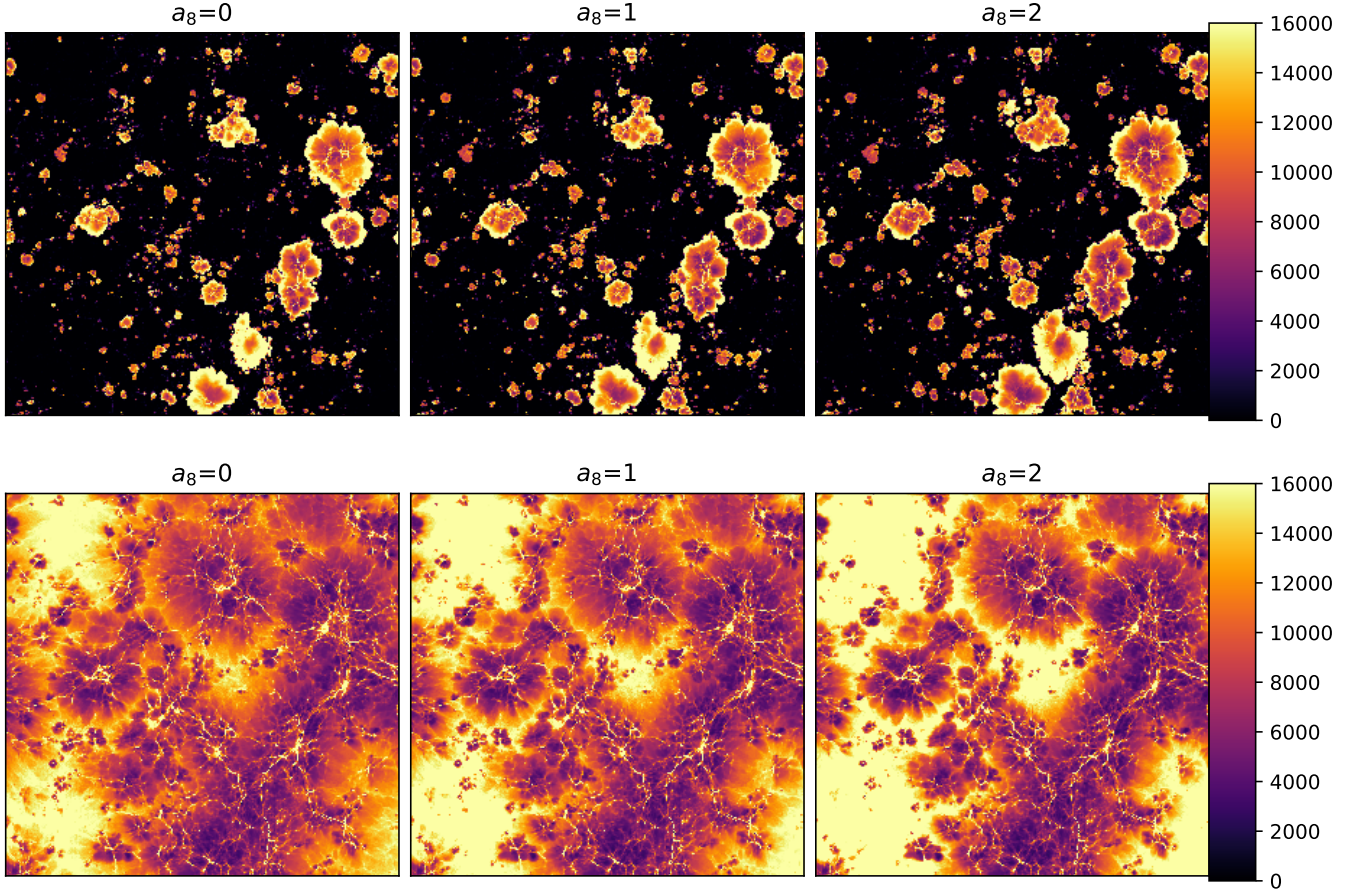


Figure 10. Image of a slice of size $(50 h^{-1} \text{Mpc})^2$ of the temperature field for our three models at $z \approx 9.5$ (top), and $z = 5.5$ (bottom).

ture is related to the duration of the reionization Δz a shorter duration leading to lesser time for the adiabatic cooling process to act and consequently to a harsher heating. However, by normalizing the temperatures by their maximum values and showing them as a function of the ionization fraction x_{HII} , it is relevant to think that the underlying photoheating process of the reionization stays the same whatever the model of escape fraction. Finally, after the ionization process, the gas starts to cool which spatially results in the fact that, at

the end of the reionization, the underdense gas regions are hotter than the overdense gas regions which were ionized earlier and had more time to cool.

We thank Francois Lanusse and Michelle Ntampaka for helpful discussions. AD acknowledges the McWilliams Center for Cosmology for hosting his internship. HT acknowledges support from NASA grant ATP-NNX14AB57G. Simulations were run at the NASA Advanced Supercomputing (NAS) Center.

REFERENCES

Adam, R., Aghanim, N., Ashdown, M., et al. 2016, *Astronomy & Astrophysics*, 596, A108

Ade, P. A. R., Aghanim, N., Arnaud, M., et al. 2016, *Astronomy & Astrophysics*, 594, A13

Aghanim, N., Ashdown, M., Aumont, J., et al. 2016, *Astronomy & Astrophysics*, 596, A107

Battaglia, N., Natarajan, A., Trac, H., Cen, R., & Loeb, A. 2013a, *The Astrophysical Journal*, 776, 83

Battaglia, N., Trac, H., Cen, R., & Loeb, A. 2013b, *The Astrophysical Journal*, 776, 81

Bolton, J. S., & Haehnelt, M. G. 2007, *Monthly Notices of the Royal Astronomical Society*, 382, 325

Bouwens, R. J., Illingworth, G. D., Oesch, P. A., et al. 2015a, *The Astrophysical Journal*, 811, 140

Bouwens, R. J., Oesch, P. A., Illingworth, G. D., Ellis, R. S., & Stefanon, M. 2017, *The Astrophysical Journal*, 843, 129

Bouwens, R. J., Illingworth, G. D., Oesch, P. A., et al. 2015b, *The Astrophysical Journal*, 803, 34

Bouwens, R. J., Oesch, P. A., Labb  , I., et al. 2016, *The Astrophysical Journal*, 830, 67

Bowler, R. A. A., Dunlop, J. S., McLure, R. J., et al. 2015, *Monthly Notices of the Royal Astronomical Society*, 452, 1817

Chen, H.-w., Prochaska, J. X., & Gnedin, N. Y. 2007, *The Astrophysical Journal*, 667, L125

Faisst, A. L. 2016, *The Astrophysical Journal*, 829, 99

Feng, Y., Di-Matteo, T., Croft, R. A., et al. 2016, *Monthly Notices of the Royal Astronomical Society*, 455, 2778

Finkelstein, S. L., Ryan, R. E., Papovich, C., et al. 2015, *The Astrophysical Journal*, 810, 71

George, E. M., Reichardt, C. L., Aird, K. A., et al. 2015, *The Astrophysical Journal*, 799, 177

Gnedin, N. Y. 2016, *The Astrophysical Journal*, 825, L17

Greig, B., & Mesinger, A. 2017, *Monthly Notices of the Royal Astronomical Society*, 465, 4838

Iwata, I., Inoue, A. K., Matsuda, Y., et al. 2009, *The Astrophysical Journal*, 692, 1287

Konno, A., Ouchi, M., Shibuya, T., et al. 2017, *Frontiers in Neural Circuits*, 10, 23

La Plante, P., Trac, H., Croft, R., & Cen, R. 2017, *The Astrophysical Journal*, 841, 87

Liu, C., Mutch, S. J., Angel, P. W., et al. 2016, *Monthly Notices of the Royal Astronomical Society*, 462, 235

Livermore, R. C., Finkelstein, S. L., & Lotz, J. M. 2017, *The Astrophysical Journal*, 835, 113

Mashian, N., Oesch, P., & Loeb, A. 2015, *Mon. Not. R. Astron. Soc.*, 000, 1

Mason, C. A., Trenti, M., & Treu, T. 2015, *The Astrophysical Journal*, 813, 21

McGreer, I. D., Mesinger, A., & D'Odorico, V. 2014, *Monthly Notices of the Royal Astronomical Society*, 447, 499

Ocvirk, P., Gillet, N., Shapiro, P. R., et al. 2016, *Monthly Notices of the Royal Astronomical Society*, 463, 1462

Oesch, P. A., Bouwens, R. J., Illingworth, G. D., Labb  , I., & Stefanon, M. 2017, arXiv:1710.11131

Ostriker, J. P., & Vishniac, E. T. 1986, *The Astrophysical Journal*, 306, L51

Ota, K., Iye, M., Kashikawa, N., et al. 2017, 6, arXiv:1703.02501

Price, L. C., Trac, H., & Cen, R. 2016, 6, arXiv:1605.03970

Schroeder, J., Mesinger, A., & Haiman, Z. 2013, *Monthly Notices of the Royal Astronomical Society*, 428, 3058

Smith, B. M., Windhorst, R. A., Jansen, R. A., et al. 2016, 6, arXiv:1602.01555

Sunyaev, R. A., & Zeldovich, Y. B. 1970, *Astrophysics and Space Science*, 7, 3

Tilvi, V., Papovich, C., Finkelstein, S. L., et al. 2014, *The Astrophysical Journal*, 794, 5

Trac, H., & Cen, R. 2007, *The Astrophysical Journal*, 671, 1

Trac, H., Cen, R., & Loeb, A. 2008, *The Astrophysical Journal*, 689, L81

Trac, H., Cen, R., & Mansfield, P. 2015, *The Astrophysical Journal*, 813, 54

Trac, H., & Gnedin, N. Y. 2011, *Advanced Science Letters*, 4, 228

Trac, H., & Pen, U.-L. 2004, *New Astronomy*, 9, 443

Zahn, O., Reichardt, C. L., Shaw, L., et al. 2012, *The Astrophysical Journal*, 756, 65

APPENDIX

A. CONVERGENCE TEST

To emphasize our guess on the f_{esc} dependency of the duration of the reionization Δz and its asymmetry Az , we hereby present our analysis of the convergence of these values by increasing the resolution.

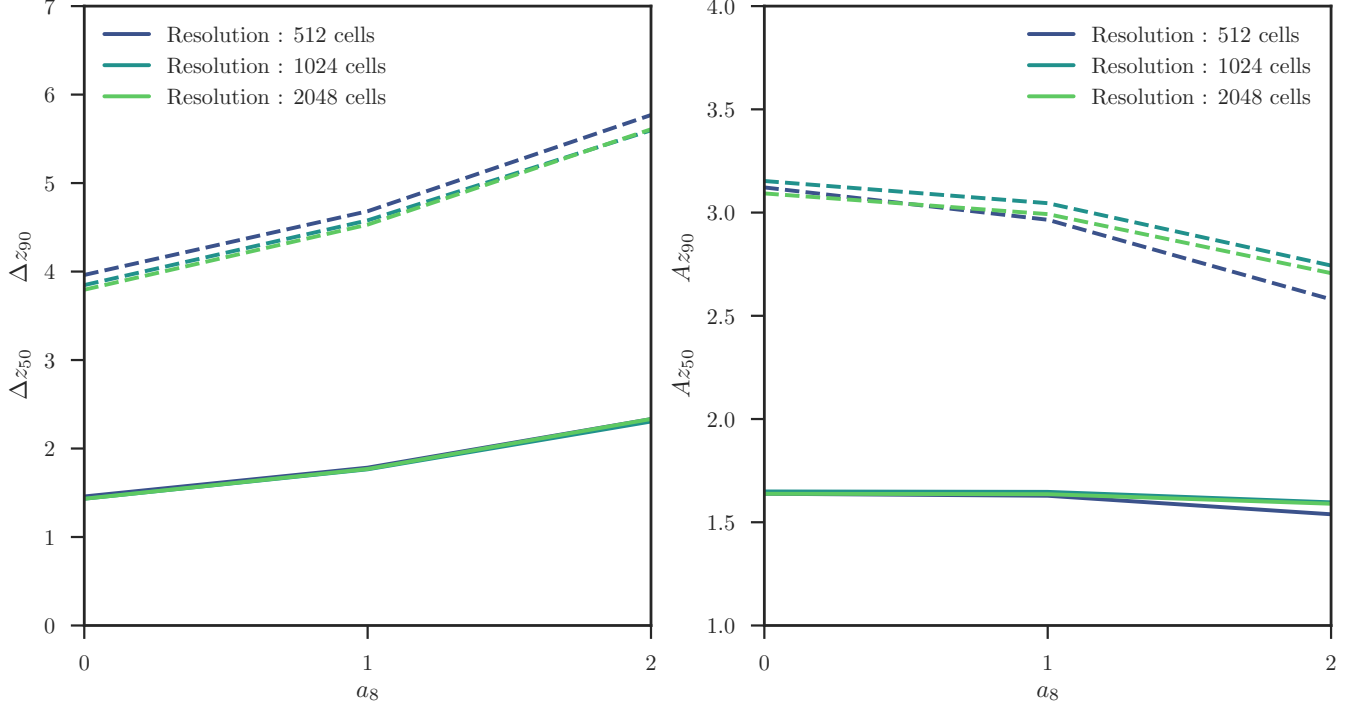


Figure 11. The characterizing values of the reionization as a function of the redshift of half ionization $z_{0.5}$ while varying the resolution of the simulation with: at left the duration of the reionization Δz_{50} (continuous) and Δz_{90} (dash) and at right the asymmetry Az_{50} (continuous) and Az_{90} (dash).

Figure 11 shows the duration of the reionization Δz and the asymmetry of the process Az depending on the resolution. As we presented it above, Δz seems to increase and Az to decrease when $z_{0.5}$ decreases. Here, we show that this conclusion does not depend on the resolution of the simulation. Moreover, especially in the case of the duration Δz , the values appear to converge to a certain limit value when the resolution increases. That fact allow us to conclude that the previously deduced dependencies are likely true and are not just a result of our limited resolution. However more studies for other values of $z_{0.5}$ and then a_8 are required to really endorse that conclusion.

B. SIMULATION RESULTS

We summarize in Table 3 the values of the main quantities obtained from SCORCH RadHydro simulation for a representative redshift set.

| z | $x_{\text{HII}, a_8=0}$ | $\frac{n_{\gamma, a_8=0}(>z)}{n_{\text{H}}}$ | $x_{\text{HII}, a_8=1}$ | $\frac{n_{\gamma, a_8=1}(>z)}{n_{\text{H}}}$ | $x_{\text{HII}, a_8=2}$ | $\frac{n_{\gamma, a_8=2}(>z)}{n_{\text{H}}}$ |
|-------|-------------------------|--|-------------------------|--|-------------------------|--|
| 13.5 | 0.002 | 0.021 | 0.005 | 0.032 | 0.01 | 0.049 |
| 13.25 | 0.003 | 0.026 | 0.006 | 0.039 | 0.012 | 0.058 |
| 13.0 | 0.004 | 0.032 | 0.008 | 0.047 | 0.015 | 0.068 |
| 12.75 | 0.005 | 0.039 | 0.01 | 0.056 | 0.018 | 0.081 |
| 12.5 | 0.007 | 0.047 | 0.013 | 0.067 | 0.022 | 0.095 |
| 12.25 | 0.009 | 0.057 | 0.016 | 0.08 | 0.027 | 0.112 |
| 12.0 | 0.012 | 0.069 | 0.02 | 0.096 | 0.032 | 0.131 |
| 11.75 | 0.015 | 0.084 | 0.024 | 0.113 | 0.039 | 0.152 |
| 11.5 | 0.019 | 0.101 | 0.03 | 0.134 | 0.046 | 0.177 |
| 11.25 | 0.024 | 0.121 | 0.037 | 0.158 | 0.055 | 0.206 |
| 11.0 | 0.031 | 0.145 | 0.046 | 0.187 | 0.067 | 0.238 |
| 10.75 | 0.04 | 0.174 | 0.057 | 0.219 | 0.079 | 0.275 |
| 10.5 | 0.05 | 0.206 | 0.069 | 0.255 | 0.093 | 0.315 |
| 10.25 | 0.062 | 0.243 | 0.083 | 0.296 | 0.109 | 0.358 |
| 10.0 | 0.077 | 0.285 | 0.1 | 0.341 | 0.127 | 0.406 |
| 9.75 | 0.095 | 0.333 | 0.118 | 0.391 | 0.146 | 0.458 |
| 9.5 | 0.116 | 0.388 | 0.14 | 0.447 | 0.168 | 0.515 |
| 9.25 | 0.141 | 0.45 | 0.165 | 0.51 | 0.191 | 0.576 |
| 9.0 | 0.171 | 0.521 | 0.194 | 0.579 | 0.218 | 0.642 |
| 8.75 | 0.209 | 0.602 | 0.228 | 0.655 | 0.248 | 0.714 |
| 8.5 | 0.254 | 0.693 | 0.268 | 0.74 | 0.281 | 0.791 |
| 8.25 | 0.309 | 0.797 | 0.314 | 0.834 | 0.318 | 0.875 |
| 8.0 | 0.375 | 0.915 | 0.367 | 0.938 | 0.359 | 0.964 |
| 7.75 | 0.456 | 1.049 | 0.43 | 1.052 | 0.404 | 1.061 |
| 7.5 | 0.553 | 1.202 | 0.503 | 1.179 | 0.456 | 1.164 |
| 7.25 | 0.667 | 1.374 | 0.586 | 1.318 | 0.512 | 1.275 |
| 7.0 | 0.798 | 1.57 | 0.682 | 1.471 | 0.574 | 1.393 |
| 6.75 | 0.931 | 1.792 | 0.789 | 1.64 | 0.643 | 1.519 |
| 6.5 | 0.998 | 2.044 | 0.903 | 1.824 | 0.718 | 1.652 |
| 6.25 | 1.0 | 2.328 | 0.985 | 2.026 | 0.799 | 1.793 |
| 6.0 | 1.0 | 2.65 | 1.0 | 2.247 | 0.886 | 1.943 |
| 5.75 | 1.0 | 3.011 | 1.0 | 2.485 | 0.96 | 2.098 |
| 5.5 | 1.0 | 3.425 | 1.0 | 2.75 | 0.999 | 2.264 |

Table 3. Characteristic quantities of the model obtained from SCORCH simulation for $a_8 = 0, 1$ and 2 .